Pionic weak decay of the lightest double-Λ hypernucleus ${}^{4}_{\Lambda\Lambda}$H

Izumi Kumagai-Fuse and Shigeto Okabe
Center for Information and Multimedia Studies, Hokkaido University, Sapporo 060-0811, Japan
(Received 31 December 2001; published 22 July 2002)

The weak π^- decay of ${}^{4}_{\Lambda\Lambda}$H is theoretically analyzed and compared with a recent BNL-E906 experiment. The two-body π^- decay width of ${}^{4}_{\Lambda\Lambda}$H is calculated to be $0.69\Gamma_\Lambda$, and its branching ratio to the total π^- decay is determined to be about 25%. The branching ratio of decay channels accompanied by a Λ particle to the total π^- decay is about 43%. The calculated π^- spectrum of ${}^{4}_{\Lambda\Lambda}$H has a broad peak around 100 MeV/c in the nuclear continuum region, whose value is inconsistent with the experimental result of a peak structure around 104 MeV/c. The other possible decays within the 104 MeV/c peak are reanalyzed, that is Λ-hypernuclear pair decays of ${}^{3}_{\Lambda}$H and ${}^{6}_{\Lambda}$He, which decay into excited states of ^{6}Li.

DOI: 10.1103/PhysRevC.66.014003 PACS number(s): 21.80.+a, 21.45.+v

I. INTRODUCTION

One of the purposes of hypernuclear studies is to reveal the properties of interactions between baryons. ΛΛ and ΞN interactions are strongly required to be determined for investigating structures of nuclear systems consisting of octet baryons, for instance, condensed matter at the center of neutron stars. A recent emulsion experiment has provided a clear evidence of ${}^{6}_{\Lambda\Lambda}$He, and has shown that the ΛΛ interaction energy of $\Delta B_{\Lambda\Lambda}$ in ${}^{6}_{\Lambda\Lambda}$He is about 1 MeV [1], which suggests that the ΛΛ interaction is weakly attractive. In order to clarify the characteristics of the ΛΛ interaction we need to accumulate experimental data and to analyze light double-Λ hypernuclei.

Recently, very intensive K^- beams have been obtained at the BNL-AGS accelerator, which produced many double-Λ hypernuclei by (K^-,K^+) and stopped Ξ^- reactions. In these reactions, weak-decay π^- particles from hypernuclei are used to identify hypernuclear species. Ahn *et al*. have reported that the momenta of two weak-decay π^- particles from $S=-2$ hypernuclei have been measured in stopped Ξ^- and (K^-,K^+) reactions on ^{9}Be in the BNL-E906 experiment [2]. In this experiment, π^- decays with specific momenta have been analyzed to come from sequential decays of ${}^{4}_{\Lambda\Lambda}$H. ${}^{4}_{\Lambda\Lambda}$H is predicted to be the lightest double-Λ hypernucleus by a theoretical calculation of a few-body system [3]. If this nucleus exists, it would certainly provide important information about the ΛΛ interaction, such as a deuteron in an *NN* interaction. The analysis in the BNL-E906 experiment was carried out based on the assumptions that there exists a narrow resonance in ${}^{3}_{\Lambda}\mathrm{H}+p$ scattering and no considerable contributions for such decays as a twin-Λ hypernuclei of ${}^{3}_{\Lambda}\mathrm{H}+{}^{6}_{\Lambda}\mathrm{He}$.

In the present paper, we discuss pionic decays of ${}^{4}_{\Lambda\Lambda}$H, while focusing on the π^- decay widths and sequential π^- decay spectra. We carefully compare the result with the BNL-E906 exprimental data and discuss the assumptions mentioned above. Yamamoto *et al.* calculated the π^- decay widths of ${}^{4}_{\Lambda\Lambda}\mathrm{H}\to{}^{4}_{\Lambda}\mathrm{He}(0^+)+\pi^-$ and ${}^{3}_{\Lambda}\mathrm{H}+p+\pi^-$, where the converted proton forms a bound state or a continuum state [4]. They have not analyzed the decay spectra of ${}^{4}_{\Lambda\Lambda}$H. Though they disregard the $({}^{2}\mathrm{H}+\Lambda)_{3/2}+p+\pi^-$ channel, which has no bound states, it should be taken into account for an overall understanding of the pionic decay of ${}^{4}_{\Lambda\Lambda}$H because the spin 3/2 configuration of ${}^{3}_{\Lambda}$H is considered to have a large probability in the initial state of ${}^{4}_{\Lambda\Lambda}$H. We therefore take the ${}^{2}\mathrm{H}+\Lambda+p+\pi^-$ decay channel into consideration.

II. FRAMEWORK

All π^- decay modes of ${}^{4}_{\Lambda\Lambda}$H are given by

$$ {}^{4}_{\Lambda\Lambda}\mathrm{H}\to{}^{4}_{\Lambda}\mathrm{He}(0^+)+\pi^-, \tag{1}$$

$$ \to{}^{4}_{\Lambda}\mathrm{He}(1^+)+\pi^-, \tag{2}$$

$$ \to{}^{3}_{\Lambda}\mathrm{H}+p+\pi^-, \tag{3}$$

$$ \to{}^{3}\mathrm{He}+\Lambda+\pi^-, \tag{4}$$

$$ \to{}^{2}\mathrm{H}+\Lambda+p+\pi^-, \tag{5}$$

$$ \to p+n+p+\Lambda+\pi^-. \tag{6}$$

The spin and parity of ${}^{4}_{\Lambda\Lambda}$H must be 1^+, because the main configuration is considered to be $[{}^{2}\mathrm{H}(1^+)\otimes\Lambda\Lambda(0^+)]_{1^+}$. Since spin-non-flip processes dominate pionic decays, process (2) dominates two-body decays, while process (1) is largely suppressed. Yamamoto *et al.* have not taken process (2) into consideration [4]. Process (6) is neglected in the present calculation, since the branching ratio is expected to be small, based on an analysis by Kamada *et al.* about the decay ${}^{3}_{\Lambda}\mathrm{H}\to p+n+p+\pi^-$, whose branching ratio to the total π^- decay is about 1% [5].

We evaluate the decay widths by an impulse approximation. For *N*-body decay,

$$\Gamma^{NB}_{\pi^-}=\frac{(\hbar c)^3}{(2\pi)^{3(N-2)+1}}\int d\vec{k}_{\pi^-}d\vec{k}_{c_1}\cdots d\vec{k}_{c_{N-1}}\frac{1}{E_\pi}\delta(E_f-E_i)$$
$$\times\delta(\vec{k}_{\pi^-}+\vec{k}_{c_1}+\cdots+\vec{k}_{c_{N-1}})\frac{1}{2J_i+1}\sum_{M_i,J_f,M_f}|\mathcal{M}_{fi}|^2, \tag{7}$$

$$\mathcal{M}_{fi} \equiv \langle \Psi_f | \left[s_{\pi^-} + i p_{\pi^-} \frac{(\vec{\sigma}\cdot\vec{\nabla}_\pi)}{k^{(0)}_{\pi^-}} \right] \chi^{(-)*}_{\pi^-} O_{\Lambda\to p} | \Psi^{\ {}^4_{\Lambda\Lambda}\mathrm{H}} \rangle, \tag{8}$$

where $\int d\vec{k}_{c_i}$ is an integral with respect to the momentum of each emitted particle with a suffix, c_i; e.g., ^{2}H by c_1, Λ by c_2, and p by c_3 for process (5). Coefficients s_{π^-} and p_{π^-} are interaction constants for spin-non-flip and spin-flip processes, respectively. The ratio $s^2_{\pi^-}:p^2_{\pi^-}$ is taken to be 0.88:0.12. The spin operator $\vec{\sigma}$ acts on a decaying hyperon, and $O_{\Lambda\to p}$ is a one-body operator which converts a Λ particle into a proton. For a pion wave function, $\chi^{(-)*}_{\pi^-}$, we take both cases of a plane wave (PW) and a distorted wave (DW) which is determined with an optical potential of the MSU group [6]. The modified parameter set 1 is used in the present calculation (see Table III and the figure caption of Fig. 5 in Ref. [6]). $\Psi^{\ {}^4_{\Lambda\Lambda}\mathrm{H}}$ and Ψ_f denote the initial- and the final-state nuclear wave functions, respectively.

The two-body pionic-decay width, $\Gamma^{2B}_{\pi^-}$, is rewritten as

$$\Gamma^{2B,J_f}_{\pi^-} = \frac{4\pi\Gamma^{(0)}_{\pi^-}}{s^2_{\pi^-}+p^2_{\pi^-}} \frac{k_{\pi^-}}{k^{(0)}_{\pi^-}} \frac{1+\dfrac{E^{(0)}_{\pi^-}}{M_p c^2}}{1+\dfrac{E_{\pi^-}}{M_{c_1}c^2}} \frac{2J_f+1}{2J_i+1} \sum_\lambda |\mathcal{M}_\lambda|^2, \tag{9}$$

$$\mathcal{M}_\lambda = \langle \Psi^{J_f}_f \| \left[s_{\pi^-} + i p_{\pi^-} \frac{(\vec{\sigma}\cdot\vec{\nabla}_\pi)}{k^{(0)}_{\pi^-}} \right] \tilde{j}_\lambda(k_\pi r_\pi) Y_\lambda(\hat{\vec{r}_\pi}) \| \Psi^{J_i}_i \rangle \equiv \frac{\langle \Psi^{J_f M_f}_f | \left[s_{\pi^-} + i p_{\pi^-} \dfrac{(\vec{\sigma}\cdot\vec{\nabla}_\pi)}{k^{(0)}_{\pi^-}} \right] \tilde{j}_\lambda(k_\pi r_\pi) Y_{\lambda\mu}(\hat{\vec{r}_\pi}) | \Psi^{J_i M_i}_i \rangle}{(J_i M_i \lambda\mu | J_f M_f)}, \tag{10}$$

where $k^{(0)}_{\pi^-}$ ($E^{(0)}_{\pi^-}$) and $\Gamma^{(0)}_{\pi^-}$ are the π^- wave number (the total energy) and a π^- decay width of a free Λ particle, respectively. The π^- decay width, $\Gamma^{(0)}_{\pi^-}$, is empirically determined to be $0.641\Gamma_\Lambda$, where Γ_Λ is the total decay width of a free Λ particle. A radial part of the π^- wave function, $\tilde{j}_\lambda(k_\pi r_\pi)$, tends to a spherical Bessel function in the plane wave (no Coulomb) limit. The other three-body and four-body decay widths are also calculated similarly.

We obtain the nuclear bound states of the initial and the final states ($^4_{\Lambda\Lambda}$H,$^4_\Lambda$He,$^3_\Lambda$H,^{3}He,^{2}H) by a variational method. The wave functions are expanded in terms of Gaussian bases with rearrangement channels in the Jacobi coordinates [7]. We take only a zero-angular momentum for each coordinate, since it is expected to be sufficient to obtain the binding energies by using central interactions [8]. The spacial coordinates used here are shown in Fig. 1.

We use an interaction by Malfliet and Tjon [9] for the NN and interactions by Akaishi *et al.* [10] for the $N\Lambda$ and $\Lambda\Lambda$ which are based on the Nijmegen D potential [11]. The values of the interaction parameters are listed in Table I. The strengths of the attractive parts are readjusted to reproduce the binding energies of nuclei and hypernuclei by factors f^{NN}_A and $f^{N\Lambda}_A$, as shown in Table II. The calculated binding energies counted from each threshold energy are also listed in Table II. We treat the $\Lambda\Lambda$ interaction strength ($f^{\Lambda\Lambda}_A$) as a parameter to understand the dependences of the π^- decay widths on the binding energy of $^4_{\Lambda\Lambda}$H.

The scattering wave functions of a $^3_\Lambda$H-p and a ^{3}He-Λ channel are obtained by solving single-channel problems with folding potentails, where we use the calculated wave functions of the bound states of $^3_\Lambda$H and ^{3}He.

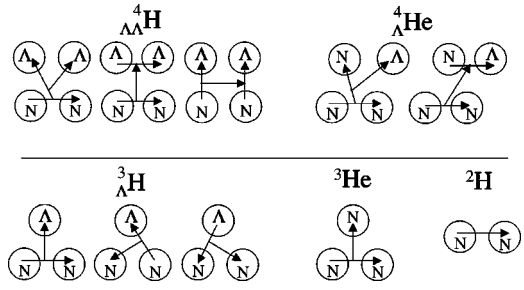

FIG. 1. Spacial coordinates adopted in variational calculations of the bound states of $^4_{\Lambda\Lambda}$H, $^4_\Lambda$He, $^3_\Lambda$H, ^{3}He, and ^{2}H. Antisymmetrized coordinates are also taken into account.

TABLE I. Interaction parameters. For NN, $V(r)=V_R e^{-\mu_R r}/r - V_A e^{-\mu_A r}/r$. For $N\Lambda$ and $\Lambda\Lambda$, $V(r)=V_R e^{-(r/\gamma_R)^2} - V_A e^{-(r/\gamma_A)^2}$. An $N\Lambda$ interaction in triplet-odd state is the averaged one with weights of $(2J+1)$ over $^3P_0$, $^3P_1$, and $^3P_2$.

NN	V_R (MeV fm)	μ_R(1/fm)	V_A (MeV fm)	μ_A (1/fm)
^3E	1458.247	3.110	635.393	1.555
^1E	1458.247	3.110	520.943	1.555
$N\Lambda$	V_R (MeV)	γ_R (fm)	V_A (MeV)	γ_A (fm)
^3E	763.11	0.5	83.938	1.2
^1E	1165.0	0.5	105.12	1.2
^3O	1862.756	0.5	44.754	1.2
^1O	272.02	0.5	31.143	1.2
$\Lambda\Lambda$				
^1E	5000.0	0.355	332.97	0.8550

TABLE II. Calculated binding energies (BE) of nuclei counted from each threshold energy in units of MeV.

	BE_{exp}	BE_{cal}	f_A^{NN}	$f_A^{N\Lambda}$	$f_A^{\Lambda\Lambda}$	Threshold
^{2}H	2.224	2.240	1.0			$p+n$
^{3}He	7.72	7.82	0.994			$p+p+n$
$^3_\Lambda$H	0.13	0.12	1.0	1.09		$d+\Lambda$
$^4_\Lambda$He(0^+)	2.39	2.31	0.994	1.1		^{3}He$+\Lambda$
$^4_\Lambda$He(1^+)	1.24	1.22	0.994	1.05		^{3}He$+\Lambda$
$^4_{\Lambda\Lambda}$H		0.30	1.0	1.09	0.8	$d+\Lambda+\Lambda$
		0.54	1.0	1.09	0.9	$d+\Lambda+\Lambda$
		1.24	1.0	1.09	1.0	$d+\Lambda+\Lambda$
		2.30	1.0	1.09	1.1	$d+\Lambda+\Lambda$

For a four-body decay to $^2\mathrm{H}+\Lambda+p+\pi^-$ we assume that the decay proceeds as follows: First a Λ particle in $^4_{\Lambda\Lambda}$H decays while keeping a part of $^3_\Lambda$H as a spectator. Next, the part of $^3_\Lambda$H breaks to scattering states of $(^2\mathrm{H}+\Lambda)_{1/2,3/2}$.

III. RESULTS AND DISCUSSIONS

A. Decay widths

The calculated decay widths of $^4_{\Lambda\Lambda}$H are summarized in Table III and Table IV in units of Γ_Λ. In order to see the dependences of the calculated two-body decay widths on the $\Lambda\Lambda$ interaction, we change the strength of the attractive part of the interaction by a factor $f_A^{\Lambda\Lambda}$. The dependence of the decay widths on the factor are also shown in Table III.

The pionic-decay width of Λ hypernuclei depends essentially on the overlap between a Λ wave function in the initial state and a proton wave function in the final state, since both the annihilation of Λ and the creation of a proton occur at the same point due to the short-range nature of the weak interaction. A Λ particle in light Λ hypernuclei is more weakly bound than nucleons. Table III shows that the two-body decay width increases with the value of $f_A^{\Lambda\Lambda}$, since the overlap between wave functions of Λ and proton become better as the bindings of $\Lambda\Lambda$ in $^4_{\Lambda\Lambda}$H become stronger.

For the *s*-shell Λ hypernuclei, distortions of pion wave functions bring about effects that two-body decay widths decrease while three-body decay widths increase [12]. The transition matrix elements of Eq. (8) decrease (increase) in two-body (three-body) decays with $s(p)$ waves of pions, since the *s* wave is pushed out by a distortion, while the *p* wave is drawn in. This is caused by a characteristic feature of a π-*N* interaction through π-nucleus optical potentials in light nuclei. This feature is expected to hold in *s*-shell double-Λ hypernuclei. Unfortunately, no π-hypernucleus optical potentials are available. In order to see the effects of the pion distortion, we evaluate two-body decay widths with an optical potential of π^--^{4}He for π^--$^4_\Lambda$He. This effect is roughly 10% as given in Table III.

TABLE III. Calculated π^- two-body-decay widths from $^4_{\Lambda\Lambda}$H are shown in the cases of PW and DW (in parentheses) in units of Γ_Λ. The maximum π^- decay momenta, $P_\pi^{3-\max}$, to the $^3_\Lambda\mathrm{H}+p+\pi^-$ channel are also listed in the unit of MeV/c.

BE($\Lambda\Lambda$) (MeV)	$f_A^{\Lambda\Lambda}$	$^4_\Lambda$He(0^+)	$^4_\Lambda$He(1^+)	$P_\pi^{3-\max}$
0.30	0.8	0.01(0.01)	0.65(0.59)	106.8
0.54	0.9	0.01(0.01)	0.68(0.62)	106.4
1.24	1.0	0.01(0.01)	0.73(0.66)	105.3
2.30	1.1	0.01(0.01)	0.76(0.67)	103.6

TABLE IV. Calculated π^- decay widths from $^4_{\Lambda\Lambda}$H shown in the cases of PW in units of Γ_Λ. The $\Lambda\Lambda$ binding energy suggested by the BNL-E906 experiment is 0.6 MeV with experimental uncertainties of about 2 MeV.

BE($\Lambda\Lambda$) (MeV)	$^4_\Lambda$He(0^+) $\Gamma_{(1)}$	$^4_\Lambda$He(1^+) $\Gamma_{(2)}$	$^3_\Lambda\mathrm{H}+p$ $\Gamma_{(3)}$	$^3\mathrm{He}+\Lambda$ $\Gamma_{(4)}$	$^2\mathrm{H}+\Lambda+p$ $\Gamma_{(5)}$
0.54	0.01	0.68	0.80	0.10	1.18

The calculated three-body and four-body π^- decay widths are given in Table IV together with the two-body widths in the PW case where the binding energy is 0.54 MeV and the three-body and four-body decay widths are the results of a spin-non-flip term with $s^2_{\pi^-}=1$. The $\Lambda\Lambda$ binding energy suggested by the BNL-E906 experiment is 0.6 MeV with experimental uncertainties of about 2 MeV [2].

The main contributions of the three-body decays come from scattering states of the relative *p* waves of the $^3_\Lambda$H-*p* and the ^{3}He-Λ channels, which exhaust 65% of the widths in each decay process. We have no resonance states in $^3_\Lambda$H-*p* scattering calculations within reasonable interaction sets, where the maximum value of the calculated phase shift is only 10 deg in a relative *p* wave of the $^3_\Lambda$H-*p* channel.

The width of a four-body decay to $^2\mathrm{H}+\Lambda+p+\pi^-$ has the largest contribution ($\sim$43%) to the total π^- decay width, which is dominated by a configuration of $[^2\mathrm{H}(1^+)\otimes\Lambda]_{(3/2)}$. This configuration is not included in the three-body decay of $^3_\Lambda\mathrm{H}+p+\pi^-$ due to an absence of the bound state of $^3_\Lambda\mathrm{H}(3/2^+)$. Two spin configurations of $^3_\Lambda$H (3/2,1/2) in the initial state of $^4_{\Lambda\Lambda}$H are mixed in a ratio of 2:1. Then, the decay strength of the $[^2\mathrm{H}(1^+)\otimes\Lambda]_{(3/2)}$ configuration in $^4_{\Lambda\Lambda}$H is mainly distributed over the four-body decay and has a large contribution.

B. Decay spectrum

Figure 2 shows the calculated π^- decay spectrum from $^4_{\Lambda\Lambda}$H in the case of a binding energy of 0.54 MeV. In this case, the π^- spectrum has two discrete peaks from two-body decays, where a large peak around $P_\pi=116.5$ MeV/c comes from process (2) and a small peak around $P_\pi=118.2$ MeV/c comes from process (1). A peak in a nuclear continuum region is located around $P_\pi=99$ MeV/c. The position of the peak shifts to a region of a larger momentum if the binding energy of $^4_{\Lambda\Lambda}$H is changed to a smaller value. This position of the peak can be shifted up to $P_\pi=100$ MeV/c at most in the case where the binding energy

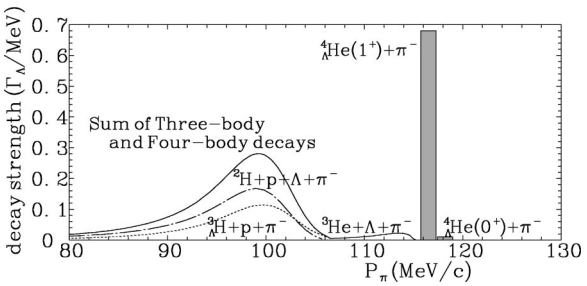

FIG. 2. π^- decay spectrum from $^4_{\Lambda\Lambda}$H. The abscissa is the π^- momentum and the ordinate is the decay strength. Each partial decay width in units of Γ_Λ is given by integrating each decay spectrum. For discrete peaks of two-body decays, the widths are presented with a width of 1 MeV as a matter of convenience, where the heights directly correspond to the decay strengths.

is equal to zero from the $^3_\Lambda$H+Λ threshold. The maximum π^- momentum to the $^3_\Lambda$H+p+π^- decay is also given in Table III.

C. Comparison with experimental data

In the BNL-E906 experiment, two π^- momenta were measured in order to observe weak-decay sequences of double-Λ hypernuclei [2]. Several peak structures were obtained on a scatter plot of the two π^- momenta, which are shown in Fig. 3 with square marks. The analysis of Ref. [2] argued that events in the most prominent peak region, $P_\pi^>$ ~114 MeV/c and $P_\pi^<$~104 MeV/c, come from sequential decays of $^4_{\Lambda\Lambda}$H, where $P_\pi^>$ ($P_\pi^<$) labels a larger (smaller) π^- momentum. The region is shown in Fig. 3 as a big open oval circle. The main sequences of π^- -weak decays from $^4_{\Lambda\Lambda}$H are summarized in Table V. The branching ratios to the total width of $^4_{\Lambda\Lambda}$H are evaluated with the calculated partial decay widths (Γ_c) of Table IV, $\mathrm{BR}_c^{1st}=\Gamma_c/\Sigma_c\Gamma_c\times 0.64$, where c denotes each decay process. We assume that nonmesonic decays of $^4_{\Lambda\Lambda}$H are negligible from the analysis on the $^3_\Lambda$H decay by Kamada *et al.* [5], where the branching ratio of nonmesonic decay is only 2%. We also assume that a π^--π^0 decay ratio of $^3_\Lambda$H ($^4_{\Lambda\Lambda}$H) is the same as that of a free Λ particle, since $^3_\Lambda$H ($^4_{\Lambda\Lambda}$H) consists of a proton, a neutron, and a (two) Λ particle(s); also, the permitted decays are symmetric between π^- and π^0 decays.

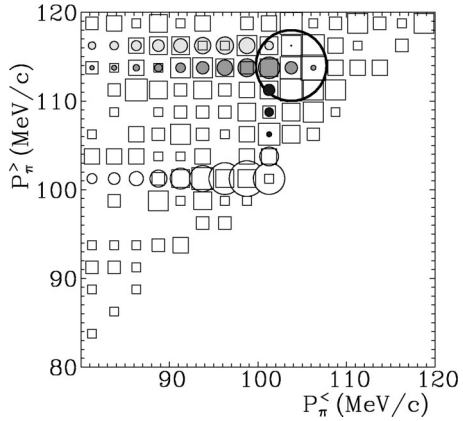

FIG. 3. Sequential π^- -decay spectrum of $^4_{\Lambda\Lambda}$H. The circles and squares show the calculated partial widths and the experimental event numbers, respectively. The light gray circle, dark gray circle, black solid circle, and open circle correspond to processes (1), (2), (4), and (5) in Table V, respectively. The region surrounded by a big open oval circle indicates the prominent peak region in the BNL-E906 experiment.

TABLE V. Main sequences of π^--weak decays from $^4_{\Lambda\Lambda}$H. Branching ratios (BR) to the total width of $^4_{\Lambda\Lambda}$H are evaluated with the calculated decay widths (Γ_c) of Table IV. Sequential-decay branching ratio is derived by multiplying BR^{1st} by BR^{2nd}.

First decays $^4_{\Lambda\Lambda}$H→	BR^{1st}	Second decays	BR^{2nd} [Ref.]
(1) $^4_\Lambda$He(1$^+$)+π^- ($P_\pi^>$~116 MeV/c)	0.16	$^4_\Lambda$He→^{3}He+p+π^- ($P_\pi^<$~96 MeV/c)	0.32 [13] [14]
(2) $^3_\Lambda$H+p+π^- ($P_\pi^<$~99 MeV/c)	0.18	$^3_\Lambda$H→^{3}He+π^- ($P_\pi^>$=114 MeV/c)	0.24 [5]
(3) $^3_\Lambda$H+p+π^- (P_π~99 MeV/c)	0.18	$^3_\Lambda$H→^{2}H+p+π^- (P_π~100 MeV/c)	0.38 [5]
(4) ^{3}He+Λ+π^- ($P_\pi^>$~113 MeV/c)	0.023	Λ→p+π^- ($P_\pi^<$~100 MeV/c)	0.64
(5) ^{2}H+Λ+p+π^- (P_π~99 MeV/c)	0.27	Λ→p+π^- (P_π~100 MeV/c)	0.64

The calculated sequential π^- decay spectrum of $^4_{\Lambda\Lambda}$H is also displayed in Fig. 3, binned in 2.5 MeV/c cells in order to be directly compared with the BNL-E906 experimental data. The cell size is proportional to each sequential decay width. The light gray circles in $P_\pi^>$~116 MeV/c correspond to two-body decays of $^4_{\Lambda\Lambda}$H→$^4_\Lambda$He(1$^+$)+π^-. The dark gray circles in $P_\pi^>$~114 MeV/c correspond to three-body decays of $^4_{\Lambda\Lambda}$H→$^3_\Lambda$H+p+π^-. The open circles in $P_\pi^>$ ~100 MeV/c correspond to four-body decays of $^4_{\Lambda\Lambda}$H →^{2}H+Λ+p+π^-.

The calculated spectrum does not show such a peak structure, as is seen in the oval region of $P_\pi^>$~114 MeV/c and $P_\pi^<$~104 MeV/c. The calculated widths are relatively larger than the experimental π^- distributions in the two-body decay region and the four-body decay region. If all of the π^- particles in the oval region originate from $^4_{\Lambda\Lambda}$H decays, the experimental signals of two-body and four-body decays from $^4_{\Lambda\Lambda}$H should also be largely shown. This suggests that decays of the other $S=-2$ hypernuclei than $^4_{\Lambda\Lambda}$H have to contribute in the oval region. Various $S=-2$ fragments (twin Λ and double Λ hypernuclei) are indeed produced by stopped Ξ^- reactions on ^{9}Be.

D. Other decay modes

Ahn *et al.* have discussed whether or not twin Λ hypernuclear decays of $^3_\Lambda$H+$^6_\Lambda$He and $^3_\Lambda$H+$^4_\Lambda$H make contributions in the oval region [2]. They took the following decay modes and concluded that the decays could not fully account for the experimental peak:

TABLE VI. Calculated π^- decay widths of ${}^{6}_{\Lambda}$He with the Cohen-Kurath (CK) shell model and the αd cluster model ^{6}Li wave functions in the unit of Γ_Λ. The corresponding π^- decay momenta are also listed in units of MeV/c.

Process ${}^{6}_{\Lambda}\mathrm{He}(1^-)\rightarrow$	width (CK)	width (αd)	P_{π^-}
${}^{6}\mathrm{Li}(1^+,T=0)_{gr}+\pi^-$	0.0056	0.0036	108.4
${}^{6}\mathrm{Li}(3^+,T=0)+\pi^-$	0.0189	0.0045	104.9
${}^{6}\mathrm{Li}(0^+,T=1)+\pi^-$	0.0087		102.7
${}^{6}\mathrm{Li}(2^+,T=0)+\pi^-$	0.0155	0.0095	101.4
${}^{6}\mathrm{Li}(2^+,T=1)+\pi^-$	0.0470		99.7
${}^{6}\mathrm{Li}(1^+,T=0)+\pi^-$	0.0066	0.0045	99.2
$\alpha+d+\pi^-$ (off resonance)		0.0017	<100
All CK waves	0.146		

$$ {}^{3}_{\Lambda}\mathrm{H}\rightarrow{}^{3}\mathrm{He}+\pi^- \quad (P^{>}_{\pi}=114\ \mathrm{MeV}/c), \tag{11} $$

$$ {}^{6}_{\Lambda}\mathrm{He}\rightarrow{}^{6}\mathrm{Li}+\pi^- \quad (P^{<}_{\pi}=108\ \mathrm{MeV}/c), $$

$$ {}^{3}_{\Lambda}\mathrm{H}\rightarrow{}^{3}\mathrm{He}+\pi^- \quad (P^{>}_{\pi}=114\ \mathrm{MeV}/c), \tag{12} $$

$$ {}^{4}_{\Lambda}\mathrm{H}\rightarrow{}^{3}\mathrm{H}+p+\pi^- \quad (P^{<}_{\pi}\sim 98\ \mathrm{MeV}/c). $$

In the π^- decay of ${}^{6}_{\Lambda}$He, there are several decay modes to the ground state of ^{6}Li and excited states of ^{6}Li. Especially, the π^- decay momenta in ${}^{6}_{\Lambda}\mathrm{He}\rightarrow{}^{6}\mathrm{Li}(J^\pi)+\pi^-$ are 104.9 MeV/c and 102.7 MeV/c for $J^\pi=3^+$ and 0^+, respectively, which correspond to the central position of the oval region. Ahn *et al.* have also mentioned that most of the decay strengths of ${}^{6}_{\Lambda}$He are expected to be below 100 MeV/c region, since the dominant decays of ${}^{6}_{\Lambda}$He are three-body ($\alpha+d+\pi^-$) decays where nuclear states are nonresonant continuum states [2].

In order to see the contributions of $\alpha+d$ nonresonant states to the ${}^{6}_{\Lambda}$He π^- decay spectrum, we calculate the partial decay widths of ${}^{6}_{\Lambda}$He, including $\alpha+d+\pi^-$ three-body decays. We found resonances of ^{6}Li at low energies with not only isospin $T=0$ ($J^\pi=1^+,3^+,2^+$), but also $T=1$ ($J^\pi=0^+,2^+$). The $T=1$ states cannot be described by $\alpha+d$ configurations. We thus use two kinds of wave functions for ^{6}Li in the present calculations: $\alpha+d$ cluster-model wave functions for $T=0$ states and Cohen-Kurath shell-model wave functions for $T=1$ states, where two-body matrix elements of (6-16)2BME are employed in view of the overall fitting to the ^{6}Li energy levels [15].

We described the wave function of ${}^{6}_{\Lambda}\mathrm{He}(1^-)$ by a single configuration of $[(0s^N_{1/2})^4(0p^n_{3/2})(0s^\Lambda_{1/2})]_{1^-}$ with harmonic oscillators, where the size parameters are determined to reproduce the calculated root-mean-square distances between α and $n(\Lambda)$ in ${}^{6}_{\Lambda}\mathrm{He}(1^-)$ by Hiyama *et al.* [16], $b_n=3.30$ fm and $b_\Lambda=2.10$ fm. We use the value $b_N=1.94$ fm for the ^{6}Li states as the oscillator strength to fit an experimental charge form factor [17].

The calculated widths and spectrum with π^- plane waves are summarized in Table VI and Fig. 4. All decays to resonance states give sizable contributions to the width of ${}^{6}_{\Lambda}$He.

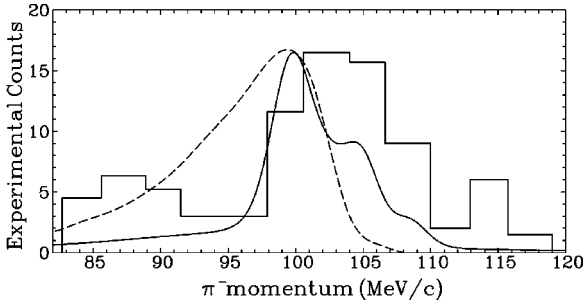

FIG. 4. Calculated π^- decay spectrum of ${}^{6}_{\Lambda}$He with the Cohen-Kurath ^{6}Li wave functions (solid line). The experimental data and the calculated ${}^{4}_{\Lambda\Lambda}$H spectrum are shown by the solid histogram and dashed line, respectively, which show the $P^{<}_{\pi}$ dependence when the other π^- momentum ($P^{>}_{\pi}$) between 107 and 119 MeV/c are summed up in Figure 3. The ordinate is the experimental count number, which is subtracted each quasi-free Ξ^--decay background shown in Ref. [2]. The calculated spectra are normalized to fit the maximum height of the experimental histogram. In the region below 100 MeV/c, there are considerable contributions from the other various decay modes, such like ${}^{3}_{\Lambda}H+{}^{4}_{\Lambda}$H.

Contributions from $\alpha+d+\pi^-$ three-body decays with nuclear nonresonant continuum states are negligible, as shown in Table VI. The widths are concentrated on these bound and resonance states in α-d relative s and d waves while small themselves in α-d relative to the p and f waves. Since a deuteron is taken to be $(0s)^2$ with an oscillator strength of $b_N=1.94$ fm in the $\alpha+d$ model, the widths are systematically smaller than those of the Choen-Kurath model due to worse overlap between the initial ${}^{6}_{\Lambda}$He and the α-d final states. However, it is sufficient within this $\alpha+d$ model in order to see qualitative contributions of nonresonant continuum α-d states to the widths.

The calculated spectrum with the Cohen-Kurath wave functions is shown in Fig. 4, which is smeared with a 3-MeV/c π^--momentum resolution with Gaussian shapes. Each width of the resonance states is also taken into account in the spectrum. The spectrum is also added to contributions from the Cohen-Kurath wave functions with no corresponding experimental resonance states, since they are expected to represent their continuum states. These contributions are smeared as the 10 MeV nuclear widths. As shown in Fig. 4, the calculated spectrum has sizable contribution in the region of 104 MeV/c on the experimental data.

E. Validity of theoretical expectations

In the BNL-E906 experiment, π^- decay particles in the region with momenta around 104 MeV/c were analyzed to come from ${}^{4}_{\Lambda\Lambda}$H [2]. The analysis was made on the following two assumptions. (1) There exists a p-wave resonance (${}^{4}_{\Lambda}$He*) in ${}^{3}_{\Lambda}$H-p scattering. π^- decays through the resonance dominate the peak in the region of 104 MeV/c. (2) Contributions from the π^- decays of ${}^{6}_{\Lambda}$He are thought to be negligible in the region of 104 MeV/c.

Concerning first assumption, we have investigated the possibility of a narrow resonance. In order to get a peak around 104 MeV/c, ${}^{4}_{\Lambda}$He is required to have a narrow reso-

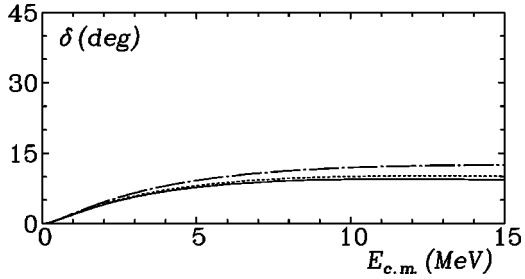

FIG. 5. The *p*-wave phase shifts for ${}^{3}_{\Lambda}$H-*p* scatterings. The solid line and the dashed (dash-dotted) line show the results calculated by the original $N\Lambda$ odd-state interactions [10], that of the attractive parts of the odd-state interactions are multiplied by 2 (5), respectively.

nance in ${}^{3}_{\Lambda}$H-*p* scattering, such as a $p_{3/2}$ resonance in α-*p* scattering of the ground state of ^{5}Li.

The $N\Lambda$ interaction strengths for even states are essentially determined by experimental binding energies of *s*-shell Λ hypernuclei, such as ${}^{3}_{\Lambda}$H, ${}^{4}_{\Lambda}$He(0^{+}), and ${}^{4}_{\Lambda}$He(1^{+}) [10]. On the other hand, those for odd states have so far hardly been determined by experimental data. We then calculated the *p*-wave phase shifts in ${}^{3}_{\Lambda}$H-*p* scatterings for the following $N\Lambda$ odd-interaction cases: (1) the original odd-state interctions [10], (2) the case that the attractive parts of the original odd-state interactions are multiplied by 2, and (3) the case that the attractive parts of the original odd-state interactions are multiplied by 5.

The results are shown in Fig. 5. Concerning the ${}^{3}_{\Lambda}$H-*p* *p*-wave scatterings, the effects of the $N\Lambda$ odd-state interactions are very weak. The maximum value of the *p*-wave phase shifts is 12° at most, even in the case (3). The $N\Lambda$ odd-state interaction strength of case (3) is the same as the ${}^{3}E$ interaction strength of the *NN* Malfliet-Tjon type, which seems to be rather attractive for the $N\Lambda$ interaction. Therefore, we have concluded to have no *p*-wave narrow resonances in the ${}^{3}_{\Lambda}$H-*p* scattering in the present framework with taking resonable changes of the $N\Lambda$ interactions into account. This framework has succeeded in explaining π^{-} decays of light Λ hypernuclei systematically [14].

The resonance has not been observed. Then, spectrum analysis of level structures of ${}^{4}_{\Lambda}$He, for instance, by ${}^{4}\mathrm{He}(K^{-},\pi^{-}p){}^{3}_{\Lambda}\mathrm{H}$ is necessary to obtain the final conclusion. Furthermore, it is noted that the position of the peak depends on the break-up threshold of ${}^{4}_{\Lambda\Lambda}$H to ${}^{3}_{\Lambda}\mathrm{H}+\Lambda$. The peak around 104 MeV/*c* is realized when the ground state of ${}^{4}_{\Lambda\Lambda}$H exists near the threshold.

Concerning the second assumption, it should be noticed that π^{-} decays of ${}^{6}_{\Lambda}$He have sizable contributions in the region of 104 MeV/*c*. The experimental counts in Fig. 4 are proportional to both the formation rates and the partial π^{-} decay rates of the hypernuclei. Though the formation rate of $({}^{9}\mathrm{Be}+\Xi^{-})_{stopped}\rightarrow{}^{3}_{\Lambda}\mathrm{H}+{}^{6}_{\Lambda}\mathrm{He}+n$ is experimentally not determined, decays from ${}^{3}_{\Lambda}\mathrm{H}+{}^{6}_{\Lambda}\mathrm{He}$ are expected to meaningfully contribute to signals in the oval region in Fig. 3. Especially, the π^{-} decays have a peak structure due to nuclear resonances of ^{6}Li in the decay of ${}^{6}_{\Lambda}$He. Therefore, the π^{-} decay spectrum of ${}^{6}_{\Lambda}$He should also be measured to distinguish the π^{-} decays of ${}^{4}_{\Lambda\Lambda}$H.

IV. SUMMARY AND CONCLUSIONS

In the present paper, we discuss the pionic-decay widths and spectra of ${}^{4}_{\Lambda\Lambda}$H and compare the calculated results with the recent BNL-E906 experimental data. The calculated width of two-body decays is $0.69\Gamma_{\Lambda}$ and the branching ratio to the total decay of ${}^{4}_{\Lambda\Lambda}$H is estimated to be about 25%. The four-body decay mode exhausts 43% of the π^{-} decay width.

The calculated spectra have only a broad peak around 100 MeV/*c*, which is inconsistent with a prominent peak of 104 MeV/*c* in the experimental data. Furthermore, although the present calculation gives comparable contributions to both two-body decays and three-body decays, the experiment has no significant peak in the region of two-body decays, unlike in the region of 104 MeV/*c*. This suggests that the other decays with $S=-2$ than ${}^{4}_{\Lambda\Lambda}$H are required to give contributions in the region of 104 MeV/*c*. Various $S=-2$ hyperfragments can be produced by a reaction of a stopped Ξ^{-} on ^{9}Be. A twin Λ-hypernuclear decay of ${}^{3}_{\Lambda}$H and ${}^{6}_{\Lambda}$He is a very possible candidate to form the peak, which decays to excited resonance states of ^{6}Li $(3^{+},0^{+},2^{+})$.

In order to establish the production of ${}^{4}_{\Lambda\Lambda}$H in the experiment, it is indispensable to make careful analyses of both the π^{-} decay spectrum of ${}^{6}_{\Lambda}$He and the level structure of ${}^{4}_{\Lambda}$He. The other exclusive productions of double-Λ hypernuclei are strongly desired, for instance, ${}^{4}_{\Lambda\Lambda}$H production via stopped Ξ^{-} on ^{4}He [18] or ${}^{5}_{\Lambda\Lambda}$H production via a Ξ-nuclear state of ${}^{7}_{\Xi}$H [19].

ACKNOWLEDGMENTS

The authors would like to express their gratitude to Professor Y. Akaishi, Professor T. Harada, and Professor T. Fukuda for fruitful discussions and comments.

[1] H. Takahashi *et al.*, Phys. Rev. Lett. **87**, 212502 (2001).
[2] J.K. Ahn *et al.*, Phys. Rev. Lett. **87**, 132504 (2001); T. Fukuda *et al.*, Nucl. Phys. **A691**, 220 (2001).
[3] S. Nakaichi-Maeda and Y. Akaishi, Prog. Theor. Phys. **84**, 1025 (1990).
[4] Y. Yamamoto, M. Wakai, T. Motoba and T. Fukuda, Nucl. Phys. **A625**, 107 (1997).
[5] H. Kamada, J. Golak, K. Miyagawa, H. Witała, and W. Glöckle, Phys. Rev. C **57**, 1595 (1998).
[6] K. Stricker, H. McManus and J.A. Carr, Phys. Rev. C **19**, 929 (1979); J.A. Carr, H. McManus and K. Stricker-Bauer, *ibid.* **25**, 952 (1982).
[7] M. Kamimura, Phys. Rev. A **38**, 621 (1988).
[8] Y. Akaishi, Int. Rev. Nucl. Phys. **4**, 259 (1986).

[9] R.A. Malfliet and J.A. Tjon, Nucl. Phys. **A127**, 161 (1969).
[10] Y. Akaishi, T. Harada, S. Shinmura, and K.S. Myint, Phys. Rev. Lett. **84**, 3539 (2000); K.S. Myint and Y. Akaishi, Prog. Theor. Phys. Suppl. **117**, 251 (1994).
[11] M.M. Nagels, T.A. Rijken, and J.J. de Swart, Phys. Rev. D **12**, 744 (1975); **15**, 2547 (1977).
[12] T. Motoba, H. Bandō, T. Fukuda, and J. Žofka, Nucl. Phys. **A534**, 597 (1991); I. Kumagai-Fuse, S. Okabe, and Y. Akaishi, *ibid.* **A585**, 365c (1995).
[13] H. Outa *et al.*, Nucl. Phys. **A585**, 109c (1995).
[14] I. Kumagai-Fuse, S. Okabe, and Y. Akaishi, Phys. Rev. C **54**, 2843 (1996).
[15] S. Cohen and D. Kurath, Nucl. Phys. **73**, 1 (1965).
[16] E. Hiyama, M. Kamimura, T. Motoba, T. Yamada, and Y. Yamamoto, Phys. Rev. C **53**, 2075 (1996).
[17] F.A. Bumiller, F.R. Buskirk, J.N. Dyer, and W.A. Monson, Phys. Rev. C **5**, 391 (1972).
[18] I. Kumagai-Fuse, S. Okabe, and Y. Akaishi (unpublished).
[19] I. Kumagai-Fuse and Y. Akaishi, Phys. Rev. C **54**, R24 (1996).